Monthly Notices of the ROYAL ASTRONOMICAL SOCIETY
MNRAS **527,** 10031–10037 (2024) https://doi.org/10.1093/mnras/stad3767

Limits of water maser kinematics: insights from the high-mass protostar AFGL 5142-MM1

Zulfazli Rosli [1,2★] Ross A. Burns [3★] Affan Adly Nazri,[1] Koichiro Sugiyama,[4] Tomoya Hirota,[5,6] Kee-Tae Kim,[7,8] Yoshinori Yonekura [9] Liu Tie,[10] Gabor Orosz [11] James Okwe Chibueze [12,13,14] Andrey M. Sobolev [15] Ji Hyun Kang,[7] Chang Won Lee,[7,8] Jihye Hwang [7] Hafieduddin Mohammad,[16] Norsiah Hashim [17] and Zamri Zainal Abidin [1★]

Affiliations are listed at the end of the paper

Accepted 2023 November 28. Received 2023 November 22; in original form 2023 August 9

ABSTRACT

Multi-epoch very long baseline interferometry (VLBI) observations measure three-dimensional water maser motions in protostellar outflows, enabling analysis of inclination and velocity. However, these analyses assume that water masers and shock surfaces within outflows are co-propagating. We compare VLBI data on maser-traced bow shocks in the high-mass protostar AFGL 5142-MM1, from seven epochs of archival data from the VLBI Exploration of Radio Astrometry (VERA), obtained from 2014 April to 2015 May, and our newly conducted data from the KVN and VERA Array (KaVA), obtained in 2016 March. We find an inconsistency between the expected displacement of the bow shocks and the motions of individual masers. The separation between two opposing bow shocks in AFGL 5142-MM1 was determined to be 337.17 ± 0.07 mas in the KaVA data, which is less than an expected value of 342.1 ± 0.7 mas based on extrapolation of the proper motions of individual maser features measured by VERA. Our measurements imply that the bow shock propagates at a velocity of 24 ± 3 km s^{-1}, while the individual masing gas clumps move at an average velocity of 55 ± 5 km s^{-1}; that is ,the water masers are moving in the outflow direction at double the speed at which the bow shocks are propagating. Our results emphasize that investigations of individual maser features are best approached using short-term high-cadence VLBI monitoring, while long-term monitoring on timescales comparable to the lifetimes of maser features is better suited to tracing the overall evolution of shock surfaces. Observers should be aware that masers and shock surfaces can move relative to each other, and that this can affect the interpretation of protostellar outflows.

Key words: masers – stars: individual: AFGL 5142-MM1 – stars: massive – ISM: jets and outflows.

1 INTRODUCTION

Because they enable us to measure proper motions in addition to local standard of rest (LSR) velocity, very long baseline interferometry (VLBI) maser three-dimensional (3D) motions are used as a kinematic tracer for several astronomical phenomena, including protostellar jets (e.g. Moscadelli et al. 2019) and expanding shells (Moscadelli et al. 2007). These 3D motions can further be used to estimate the inclination of bipolar jets (Sahai et al. 2002), the dynamical timescales of protostellar ejections (Boekholt et al. 2017), and jet rotation (Moscadelli et al. 2007). They are also used to estimate total 3D velocities of star-forming regions (SFRs), which are subsequently used in investigations of Galactic dynamics in the Milky Way, allowing substantially more accurate estimates of the Galactic constants (i.e. the solar–Galactocentric distance R_0, Galactic circular rotation velocity Θ_0, and the LSR angular rotation velocity Ω_0). Despite the proficiency and currently unique capability of VLBI maser observations for these purposes, a caveat remains in the assumption that maser 3D motions truly trace the motions of the phenomena with which they associate. However, there can be some discrepancy between the motions of individual maser cloudlets and the shocks or gas flows in which they reside. Another feasible complication to this assumption is the case where there exists a motion of the excitation conditions that give rise to maser emission rather than the gas itself, as was recently seen in the case of 6.7-GHz methanol masers (Moscadelli et al. 2017; Burns et al. 2020).

There are considered to be two dominant pumping mechanisms that give rise to maser emission: those that are predominantly pumped by radiation, and those that are predominantly pumped by collisional energy. Radiatively pumped masers such as 6.7-GHz methanol masers are typically found near a heat source (Zheng & Ling 1997; Ouyang et al. 2019), and are reasonably good tracers of motion of their hosting gas (Green & McClure-Griffiths 2011). On the one hand, cases of sudden changes to the radiative environment leading to drastic redistribution of such masers, as mentioned above, are exceptions. On the other hand, collisionally pumped masers, such as water masers, are usually found in shock regions (Hollenbach, Elitzur & McKee 2013). Such turbulent environments may give rise

★ E-mail: zulfazli.rosli@gmail.com (ZR); ross.burns@riken.jp (RAB); zzaa@um.edu.my (ZZA)

to situations where relative motions between gas flows, the maser cloudlets in those gas flows, and the shock regions provide the collisions required to pump the masers (Strelnitsky 1980; Strelnitski et al. 2002; Sobolev, Watson & Okorokov 2003). This scenario has the potential to lead to inaccurate estimates of jet motions, inclinations and dynamic timescales, and the other maser-traced phenomena mentioned above.

Episodic accretion will trigger episodic ejections (Corcoran & Ray 1998), and these ejections are visible via the formation of maser bow shocks, which show the history of accretion events occuring during the formation of massive stars (Caratti o Garatti et al. 2015). Tracing back the ejection history is an indirect way of investigating episodic accretion. This is done by measuring the velocity of these maser bow shocks, allowing the deduction of its dynamic timescale, which is basically the age of the ejection.

Maser velocities have often been assumed to give a good approximation towards the jet velocities (Goddi et al. 2005). This study aims to evaluate the validity of the above assumption, which has important consequences for the use of maser VLBI-determined dynamic timescales of ejections when inferring the accretion history of a high-mass protostar.

The massive SFR, AFGL 5142, has an abundance of outflows on multiple scales (Burns et al. 2017). It embeds two dominant 9-mm cores, MM1 and MM2, which exhibit hot core chemistry (Zhang et al. 2007). MM1 has a mass of 6.5 $M_\odot$ (Liu et al. 2016) and embeds a massive star traced by 6.7-GHz methanol masers, which detect an in-falling disc (Goddi, Moscadelli & Sanna 2011). The annual parallax of AFGL 5142 was measured to be $\pi = 0.467 \pm 0.010$ mas, corresponding to a trigonometric distance of $D = 2.14^{+0.051}_{-0.049}$ kpc (Burns et al. 2017). AFGL 5142-MM1 has a double bow shock structure, which is rare in massive SFRs and enables the evaluation of both the shock propagation and maser velocities. In addition, the source has experienced multiple previous episodes of protostellar ejections, which imply that the star has formed by episodic accretion (Burns et al. 2017). The designated masers tracing the evolution of the previously detected north-west (NW) and south-east (SE) bow shocks from Burns et al. (2017) were identified. In addition, some masers were detected further north from the bright NW bow shocks. Observations by Burns et al. (2017) were conducted between 2014 April 21 and 2015 May 29, in seven epochs.

2 OBSERVATIONS

Observations were carried out with the KVN and VERA array (KaVA) on 2016 March 21 as part of the Large Programme for star formation studies (Kim et al. 2018), a united research programme pioneered by the Korea Astronomy and Space Science Institute (KASI) and the National Astronomical Observatories of Japan (NAOJ). The observations comprised alternating scans between the target maser, AFGL 5142-MM1, and a delay calibrator, DA193, at roughly hourly intervals. A total of 6 hr 20 min of KaVA observations were conducted, which included 1 hr 54 min of integration on AFGL 5142-MM1. The beams' recorded signals are of left-hand circular polarization at all seven KaVA observatories. Each station recorded data with a total bandwidth of 256 MHz, which was sampled into 16 baseband channels using the Octave system (Oyama et al. 2011). We adopted 22.235080 GHz as the rest frequency of the water maser. A radio frequency range of one baseband channel containing the maser emission was set carefully to cover all the maser spectral components based on calculations of Doppler shift at each observation date.

Data were collected and correlated at the Korea Japan Correlation Centre (KJCC; Lee et al. 2015). Data from the Korean antennas did not produce useful correlated visibilities and were necessarily flagged. The phase tracking centre for AFGL 5142-MM1 was set at $(\sigma,\ \delta)_{J2000.0} = (5^h30^m48^s.000,\ +33°47'54''.000)$. The 16-MHz baseband channel, which included the water maser emission, was correlated with a channel separation of 7.8125 kHz, which corresponds to a velocity spacing of 0.11 km s^{-1}.

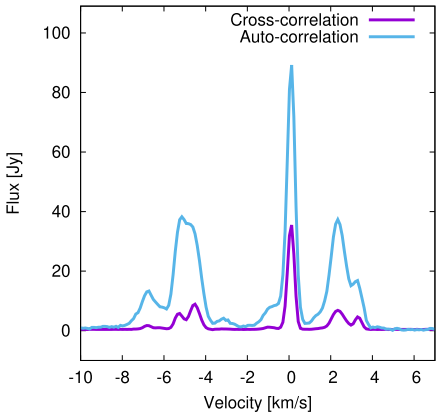

Figure 1. Cross-correlated and autocorrelated spectra of maser emission in AFGL 5142-MM1 observed using KaVA on 2016 March 21. The systematic velocity of the SFR is −1.1 km s^{-1}.

3 DATA REDUCTION

The KaVA data were reduced via the astronomical image processing system (AIPS), established by the National Radio Astronomy Observatory. Gain curve and system temperature information recorded at each station was used to apply a priori gain calibration. Delay calibration was performed on a bright source, DA193, the solutions of which were then applied to the maser data. We solved residual phase and rate differences on each baseline using the AIPS task FRING, solving on one of the brightest channels in the maser emission (avoiding the brightest channel, which exhibited a complex structure), thus self-calibrating the spectral line data.

Maser emission was imaged using the AIPS task IMAGR, employing a pixel size of 0.1 × 0.1 mas^2 and a map size of 1024 × 1024 pixel^2, which produced a map covering 0.1024 × 0.1024 arcsec^2 centred on the area around the location of reference maser (Burns et al. 2017). We also searched a 600 × 600 mas^2 region around the reference maser to ensure that all maser emission was imaged. We produced an image cube from the velocity ranges of 3.86−6.99 km s^{-1}. The image noise (rms) measured from an emission-free region in a single channel map was 160 mJy.

Water maser emission was elucidated from the image cube via the automated SAD routine in AIPS, which filters out candidate emission at a signal-to-noise ratio limit of 7. These 'spots' represent the peak emission of an individual maser in a single channel, and they are grouped into 'features', which infers that they originate from the same physical maser cloud.

4 RESULTS

4.1 Spectral profile

Fig. 1 shows the detected flux density differences between cross-correlated and autocorrelated spectra of the water masers observed with KaVA on the 2016 March 21, and Fig. 2 illustrates the spotmap

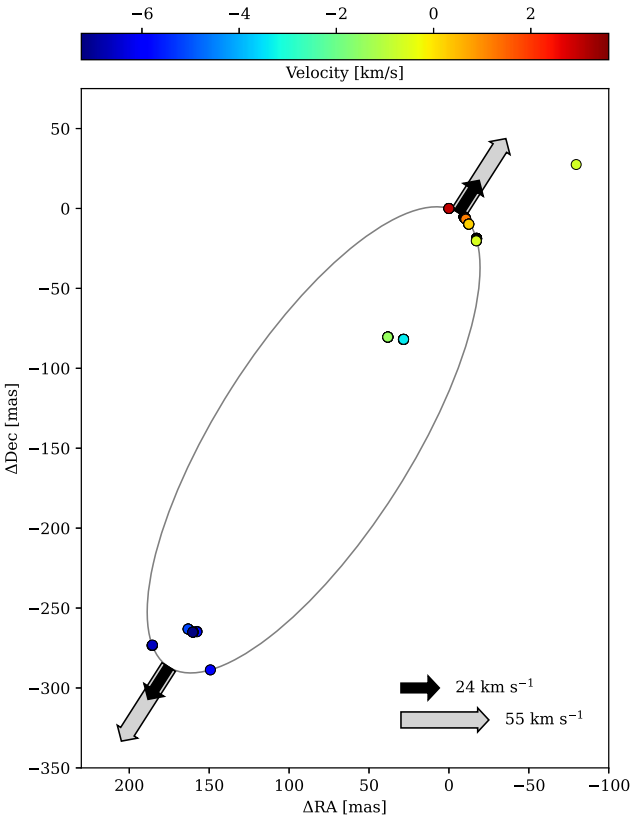

Figure 2. Spotmap of the maser emission in AFGL 5142-MM1 observed using KaVA on 2016 March 21. The grey ellipse shows the fit to the masers tracing the bow shock (see Section 4.3). The black vectors show the propagation speed of the bow shocks (this work, see Section 5.2) while grey vectors indicate the average proper motions of the maser spots associated with the same bow shocks, reported in Burns et al. (2017).

of the water masers in AFGL 5142-MM1. The spectral profiles illustrate a high degree of consistency between both correlations, with more than 50 per cent of the maser emissions resolved out. This furthermore implies an abundance of information that could be explored in the extended scale ($\gg$1 mas) maser emissions in AFGL 5142-MM1.

The KaVA observation on 2016 March 21 (see Figs 1 and 2) shows that the detected water masers have velocities ranging from 3.86 to 6.99 km s^{-1}. The line-of-sight velocity of the region was established as -1.1 km s^{-1} (Zhang et al. 2007) with the aforementioned NW and SE masers redshifted and blueshifted, respectively (Burns et al. 2017). This is consistent with Fig. 1 where the NW maser bow shocks are furthermore redshifted by approximately 4 km s^{-1} and the SE masers by about 4 km s^{-1} from the SFR systematic velocity. These clusters of maser bow shocks indicate symmetry in both the spatial and spectral domains.

It should be noted that similarities in the spectra of this work and Burns et al. (2017) indicate that masers associated with millimetre cores other than MM1 were detected by KaVA; however, as they do not contribute to the primary goal of this work, we did not process their data for imaging.

4.2 Spatial distribution

The masers associated with AFGL 5142-MM1 have an extent of about 300 × 350 mas, which is more extended than the distribution reported in Burns et al. (2017). There were 91 maser spots detected, extended in a linear distribution orientated NW–SE. Most of the masers detected by KaVA associate with the known bow shock structures in this region. The presence of persistent and newly formed maser spots is apparent.

While at first glance the maser distributions in this work resemble those from Burns et al. (2017), a closer look reveals that while the shock fronts themselves have persisted, the individual maser features have moved. This is evident in the lower left and right enlarged sections in Fig. 3. While some of the maser features appear to have persisted across the time between observations (2015 to 2016), several others have disappeared and new maser features have appeared in other parts of the shock fronts. This is not surprising as the shock-driven water masers are known to have shorter lifetimes of a year or so (Felli et al. 2007) compared with the radiatively driven Class II methanol masers, for example. Thus, the shock front structure remains a persistent feature emanating from MM1, whereas the individual maser emitting regions are transient visitors that form, disappear, and reform in various parts of the shock front.

4.3 Estimating bow shock displacement

Our main objective in this work is to investigate whether the motion of the masers is a suitable tracer for the motion of the shock front itself. This can be determined by investigating whether or not the maser features are moving through the shock or with it. In the latter case, the locations of successive generations of maser features can be determined by the proper motion of the previous generation, as both the masers and the shock region itself should be comoving. However, if the masers are moving through a shock region (in either a positive or negative velocity relation), then subsequent generations of maser features will appear displaced from their expected locations based on the trajectories of the prior generation of masers. On one extreme, considering a static shock region, individual masers will exhibit a proper motion, but long-term VLBI monitoring will reveal that subsequent generations of masers are consistently produced at the same location before traversing the shock region and eventually disappearing. Given that maser emission traces shock regions, and given enough time between observations for a new generation of maser features to be produced, the two scenarios above can distinguished by a comparison between the translocation of the shock structures over the given time period, and their expected translocation based on the proper motions of masers they host.

To investigate any discrepancy between the predicted and actual locations of the shock regions, we produced a synthetic spotmap in which the maser spots observed in 2015 May were extrapolated to their expected positions to 2016 March, based on their measured proper motions from Burns et al. (2017). This represents the expected location of the shock front in 2016 March, assuming that the maser and the shock are comoving. We then compared this to the data taken in this work, which give the actual location of the shock front in 2016 March. The separation distance of the shock fronts then reveals how far they have propagated in the sky plane in the given time.

In order to determine how far apart the NW and SE maser shock fronts have separated between the VERA (2015 May) and KaVA (2016 March) observations, in addition to their expected separation based on proper motion trajectories, we fit ellipses to the maser spot distribution using a modified version of the procedure used in Burns et al. (2017). Because the KaVA observations did not use phase referencing, we fitted ellipses to each data set to derive its centre, and then shifted each data set to a common origin. After doing so,

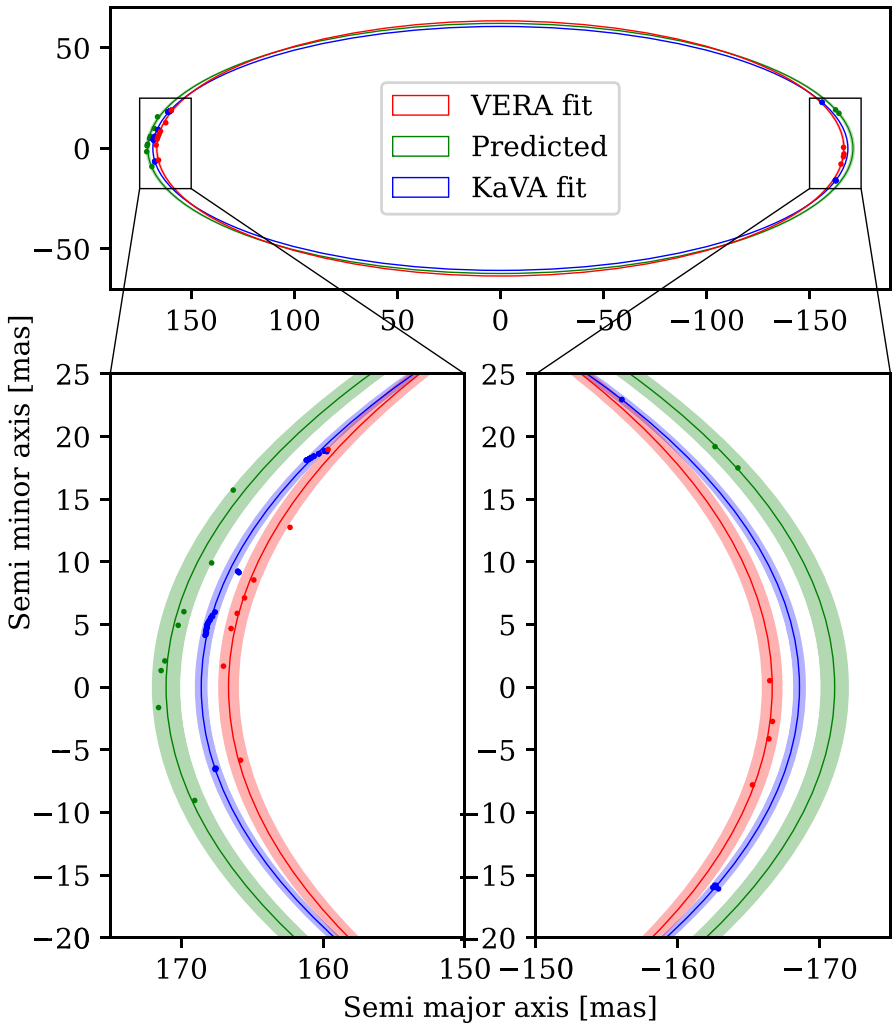

Figure 3. Comparison between the maser positions in VERA (2015 May), the predicted positions, and in KaVA (2016 May), along with their fitted ellipses. The positions in this plot are relative; that is, for each set of data, the maser positions are translated with respect to their cente, then rotated about the centre based on their rotation angle (original values shown in Table 1). The enlarged section on the lower left shows the NW region, and that on the lower right shows the SE region. Note that any masers not associating with the bow shocks, and thus not included in this analysis, were omitted from the figure.

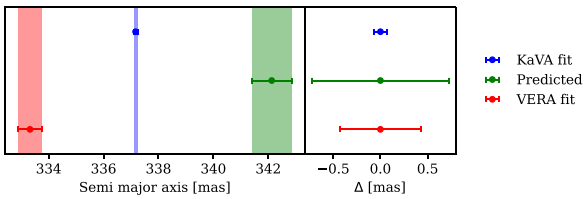

Figure 4. Visualization of the separation and their errors for each set of data. The left plot shows their values and error ranges, and the right plot shows a comparison between each set's error values.

the separation of the NW and SE bow shocks were determined by the semimajor axis of the ellipses for each corresponding spotmap, and the motion in each direction is half of the semimajor axis expansion as a function of time. Comparing the separation of the maser bow shocks as a function of time avoids the complication of considering the source systemic motion in the sky plane, thereby reducing the number of variables.

The results are as follows. The separation between the NW and SE shock regions was 333.3 ± 0.6 mas in 2015 May. Based on maser trajectories, the separation in 2016 March was expected to be 342 ± 1.4 mas. The separation of the bow shocks in this work was determined to be 337.2 ± 0.2 mas. In Fig. 3, we show an expansion of the maser distribution in the NW shock front showing the maser distributions and the determined shock region locations represented by the fitted ellipses (shown in grey with a width corresponding to the typical astrometric error adopted for VERA and KaVA observational results; Niinuma et al. 2015). Table 1 shows the fit parameters of the ellipses for each set of data. Table 2 shows the separation of the NW and SE bowshocks and their errors and Fig. 4 illustrates this visually.

It can be seen that the shock front detected via KaVA in these observations, delineated by the locations of a new generation of masers, does not move as far as is expected (predicted locations) in the 10 months between the two VLBI data sets.

Table 1. Fit parameters for the ellipses for each set of data. The fitting was performed using numerically stable direct least squares, with the errors estimated by minimization of the χ^2 function (further verified using bootstrapping).

	Centre x (mas)	Centre y (mas)	Rotation angle (rad)	Semimajor axis (mas)	Seminor axis (mas)
VERA fit	61.6 ± 0.2	-101.0 ± 0.2	2.1789 ± 0.0003	166.7 ± 0.2	63 ± 2
Predicted	71.2 ± 0.5	-98.0 ± 0.5	2.2545 ± 0.0006	171.1 ± 0.4	62 ± 2
KaVA fit	84.65 ± 0.06	-144.78 ± 0.08	2.13877 ± 0.00007	168.58 ± 0.04	60.7 ± 0.1

Table 2. Separation between the NW and SE bow shocks and their errors for each set of data.

	Separation (mas)
VERA fit	333.3 ± 0.4
Predicted	342.1 ± 0.7
KaVA fit	337.17 ± 0.07

5 DISCUSSION

5.1 Maser proper motion versus shock propagation

Multi-epoch VLBI observations can trace the proper motions of maser emission in the sky plane. In conjunction with this, consideration of the LSR velocity gives a 3D description of the spatial motion of the masers. This technique has been utilized in tracing the dynamics of star formation from the parameters obtained via analysis of ejections (see, for example, Goddi et al. 2005).

It is assumed that the measured motions of masers accurately trace the motion of the maser emitting gas, which in the case of shock-tracing water masers would presume that the 3D motion of the masers would be equal to the 3D motion of the shock region. Theoretically, we could obtain physical quantities such as the jet inclination from this information by the ratio of the line-of-sight and sky-plane velocities. The jet inclination is crucial in understanding the production and dynamical ages of protostellar outflows in addition to determining the rotation axis inclination of accretion discs. A few hypotheses for jets in massive young stellar objects include an extension of low-mass protostars as classical-disc wind, and/or external collimation of a wide-angle wind (Carrasco-González et al. 2021).

Our results have shown that discrepancies may exist between the motions of the shock and the motions of the masers. This brings into question this assumption; that is, masers may not always precisely trace the motions of the shock. This could be due to a relative motion between the propagating shock and the maser cloudlets propagating with or within the shock region, or supersonic turbulence that occurs in the gas after the shock has left the cloudlets, which gives rise to collisionally pumped maser emissions (Strelnitski et al. 2002) Ultimately, this observed effect can be attributed to the changing pumping conditions within the shock, and this depends on the physical environment and thus could vary for different sources.

It should be stressed that we do not negate the utility of masers as an estimate of the geometric and kinematic attributes of shocks but rather highlight a limitation in this approach. Indeed, there are confirmed cases where the shock motion and the motions of associated maser cloudlets are consistent (Goddi et al. 2007; Burns et al. 2016; Hirota et al. 2021). However, the determination of any corresponding parameters such as ejection rates, based on the proper motions of the masers should be done with caution. Increasing the number of motion comparison studies with observational time baselines of decades would confirm our findings to a higher degree of confidence, in addition to exploring the question of why some masers do or do not trace well to the motion of the shock regions in which they form. Such VLBI monitoring investigations would allow ample time for several generations of water masers to form, traverse, disperse, and be replaced by subsequent generations of masers. Our hope is to build upon the understanding of this topic by extending and repeating the study presented in this publication.

5.2 Deceleration of shocks

Another perspective to look into based on our results is the fact that the shock itself may slow down. It has been known that the medium around massive young stellar objects is inhomogeneous, with the strongest evidence being the presence of spiral arms in their accretion disc (Burns et al. 2023). Molecular line observations such as HNCO also agree with the presence of denser regions in molecular outflows or shocks (Xie et al. 2023). The shock would naturally slow down when it meets a denser part of the circumstellar medium.

Multiple ejection events can also produce the same result. Bow shocks from previous ejections can excavate an outflow cavern to produce a less dense region in the circumstellar medium. A secondary shock can then propagate faster in this region, approaching the slower initial/primary bow shocks. The secondary shock would then slow down as it interacts with the primary bow shocks (Meyer et al. 2020). However, considering that the physical difference between the old and new masing fronts is only 4 au, it may be more reasonable to interpret our results as shock front propagation rather than multiple ejections.

The presence of multiple jets that are linked to jet precession can also produce wide-angle shocks with inconsistent velocities, but this should affect the maser spatial distribution rather than its velocities, and its effects in AFGL 5142 have only been seen at a much larger scale (Liu et al. 2016).

Non-linear velocities are also seen in different astrophysical objects, namely the BX Cam envelope, a circumstellar envelope around a Mira variable star (Xu et al. 2022). Water maser velocities in the source were seen to not be constant based on the asymmetric spatial and velocity distributions in the maser features. The authors managed to quantify maser acceleration too, albeit the values are within uncertainties.

Nonetheless, the shock velocities predicted based on the 3D velocities using the VERA observation is $55 \pm 5\,\mathrm{km\,s^{-1}}$, whereas the KaVA data correspond to a shock velocity of $24 \pm 3\,\mathrm{km\,s^{-1}}$.

6 CONCLUSION

The short-term positional monitoring (i.e. time-scale life span of the water maser) will give a lower limit on the shock velocity. Then the long-term monitoring (several life spans of water masers) will reveal

the true motion of the shock. If both reveal the same velocity, then both the shock and the jet are moving together.

While water masers are useful tools for tracing the spatial kinematics of jets, in protostars caution should be exercised when making assumptions on how accurately/closely the 3D kinematics of masers observed via VLBI trace the true physical motion of the shock regions in the jet.

We conclude that the 3D velocity of masers may not accurately give all the information about the jet. Short-term and long-term VLBI monitoring will investigate different parts of the outflow, either the maser themselves or the shock. This work has compared both short-term (VERA) and long-term (KaVA) observations and our theory holds true.

ACKNOWLEDGEMENTS

ZR acknowledges the support provided by UM's Faculty of Science grant (GPF081A-2020), which has enabled the completion of this research and the publication of its findings. TH is supported by the MEXT/JSPS KAKENHI Grant Numbers 17K05398 and 20H05845. TL acknowledges supports from the National Key Research and Development Programme of China (No. 2022YFA1603101); the National Natural Science Foundation of China (NSFC), through grants No. 12073061 and No. 12122307; the international partnership programme of the Chinese Academy of Sciences, through grant No. 114231KYSB20200009; and the Shanghai Pujiang Programme 20PJ1415500. CWL is supported by the Basic Science Research Programme through the National Research Foundation of Korea (NRF) funded by the Ministry of Education, Science and Technology (NRF-2019R1A2C1010851), and by the Korea Astronomy and Space Science Institute grant funded by the Korea government (MSIT) (Project No. 2023-1-84000). AMS was supported by Ministry of Science and Higher Education of the Russian Federation (state contract FEUZ-2023-0019).

DATA AVAILABILITY

The data underlying this article can be accessed from KaVA's data archives under the experiment code k16th01b at https://radio.kasi.re.kr/arch/search.php.

REFERENCES

Boekholt T., Stutz A., Fellhauer M., Schleicher D., Carrillo D., 2017, MNRAS, 471, 3590
Burns R. A., Handa T., Hirota T., Motogi K., Imai H., Omodaka T., 2016, A&A, 586, A34
Burns R. A. et al., 2017, MNRAS, 467, 2367
Burns R. A. et al., 2020, Nature Astron., 4, 506
Burns R. A. et al., 2023, Nature Astron., 7, 557
Caratti o Garatti A., Stecklum B., Linz H., Lopez R. G., Sanna A., 2015, A&A, 573, A82
Carrasco-González C., Sanna A., Rodríguez-Kamenetzky A., Moscadelli L., Hoare M., Torrelles J. M., Galván-Madrid R., Izquierdo A. F., 2021, ApJ, 914, L1
Corcoran M., Ray T. P., 1998, A&A, 331, 147
Felli M. et al., 2007, A&A, 476, 373
Goddi C., Moscadelli L., Alef W., Tarchi A., Brand J., Pani M., 2005, A&A, 432, 161
Goddi C., Moscadelli L., Sanna A., Cesaroni R., Minier V., 2007, A&A, 461, 1027
Goddi C., Moscadelli L., Sanna A., 2011, A&A, 535, L8
Green J. A., McClure-Griffiths N. M., 2011, MNRAS, 417, 2500
Hirota T., Cesaroni R., Moscadelli L., Sugiyama K., Burns R. A., Kim J., Sunada K., Yonekura Y., 2021, A&A, 647, A23
Hollenbach D., Elitzur M., McKee C. F., 2013, ApJ, 773, 70
Kim K-T. et al., 2018, Proc. Int. Astron. Union, 13, 259
Lee S-S. et al., 2015, J. Korean Astron. Soc., 48, 125
Liu T. et al., 2016, ApJ, 824, 31
Meyer D. M.-A., Vorobyov E. I., Elbakyan V. G., Eislöffel J., Sobolev A. M., Stöhr M., 2020, MNRAS, 500, 4448
Moscadelli L., Goddi C., Cesaroni R., Beltrán M., Furuya R., 2007, A&A, 472, 867
Moscadelli L. et al., 2017, A&A, 600, L8
Moscadelli L., Sanna A., Goddi C., Krishnan V., Massi F., Bacciotti F., 2019, A&A, 631, A74
Niinuma K., Lee S-S., Kino M., Sohn B. W., 2015, Publ. Korean Astron. Soc., 30, 637
Ouyang X-J., Chen X., Shen Z-Q., Yang K., Li X-Q., Chen H-Y., Zhao Z., Sobolev A. M., 2019, ApJS, 245, 12
Oyama T., Mizuno S., Kono Y., Kawaguchi N., 2011, in 2011 XXXth URSI General Assembly and Scientific Symposium. URSI, p.1,
Sahai R., Brillant S., Livio M., Grebel E., Brandner W., Tingay S., Nyman L., 2002, ApJ, 573, L123
Sobolev A. M., Watson W. D., Okorokov V. A., 2003, ApJ, 590, 333
Strelnitski V., Alexander J., Gezari S., Holder B. P., Moran J. M., Reid M. J., 2002, ApJ, 581, 1180
Strelnitsky V. S., 1980, in Andrew B. H.ed., Proc. IAU Symp. Vol. 87, Interstellar Molecules. Kluwer, Dordrecht, p.591
Xie J. et al., 2023, ApJ, 949, 89
Xu S. et al., 2022, ApJ, 941, 105
Zhang Q., Hunter T. R., Beuther H., Sridharan T. K., Liu S-Y., Su Y-N., Chen H-R., Chen Y., 2007, ApJ, 658, 1152
Zheng X-W., Ling Z-F., 1997, Chinese Astron. and Astrophys., 21, 443

[1]*Department of Physics, Faculty of Science, Universiti Malaya, 50603, Kuala Lumpur, Malaysia*
[2]*CFLMS, International University of Malaya Wales, Kuala Lumpur, Malaysia*
[3]*RIKEN Cluster for Pioneering Research, 2-1 Hirosawa, Wako-shi, Saitama, 351-0198, Japan*
[4]*National Astronomical Research Institute of Thailand (Public Organization), 260 Moo 4, T. Donkaew, A. Maerim, Chiangmai, 50180 Thailand*
[5]*Mizusawa VLBI Observatory, National Astronomical Observatory of Japan, Hoshigaoka 2-12, Mizusawa, Oshu, Iwate 023-0861, Japan*
[6]*The Graduate University for Advanced Studies, SOKENDAI, 2-21-1 Osawa, Mitaka, Tokyo 181-8588, Japan*
[7]*Korea Astronomy and Space Science Institute, 776 Daedeokdae-ro, Yuseong-gu, Daejeon 34055, Republic of Korea*
[8]*University of Science and Technology, Korea (UST), 217 Gajeong-ro, Yuseong-gu, Daejeon 34113, Republic of Korea*
[9]*Center for Astronomy, Ibaraki University, 2-1-1 Bunkyo, Mito, Ibaraki 310-8512, Japan*
[10]*Shanghai Astronomical Observatory, Chinese Academy of Sciences, 80 Nandan Road, Shanghai 200030, People's Republic of China*
[11]*Joint Institute for VLBI ERIC, Oude Hoogeveensedijk 4, 7991 PD Dwingeloo, The Netherlands*
[12]*Department of Mathematical Sciences, University of South Africa, Cnr Christian de Wet Rd and Pioneer Avenue, Florida Park, 1709, Roodepoort, South Africa*
[13]*Centre for Space Research, Physics Department, North-West University, Potchefstroom 2520, South Africa*

[14]*Department of Physics and Astronomy, Faculty of Physical Sciences, University of Nigeria, Carver Building, 1 University Road, Nsukka 410001, Nigeria*
[15]*Ural Federal University, 19 Mira Street, 620002 Ekaterinburg, Russia*
[16]*Department of Astronomy, University of Tokyo, 2 Chome-21 Osawa, Mitaka, Tokyo 181-0015, Japan*
[17]*Mathematics Division, Centre for Foundation Studies in Science, Universiti Malaya, 50603, Kuala Lumpur, Malaysia*

This paper has been typeset from a TEX/LATEX file prepared by the author.